PHYSICAL REVIEW B VOLUME 31, NUMBER 8 15 APRIL 1985

Properties of fluorinated glow-discharge amorphous silicon

M. Janai, R. Weil, and B. Pratt
Department of Physics and Solid-State Institute, Technion—Israel Institute of Technology, Haifa 32000, Israel
(Received 13 September 1984)

Amorphous silicon films were prepared by plasma decomposition of SiF_4+SiF_2 gas. Structural analysis, electronic-transport-property measurements, optical-property measurements, and electron-spin-resonance measurements were performed as a function of deposition and annealing temperature. Hydrogenated amorphous silicon (*a*-Si:H) samples were prepared in a separate identical reactor under similar plasma conditions for reference. The results indicate that compensation of dangling bonds by fluorine alone can be obtained, yielding ESR values of the order of 10^{17} spins/cm^3. The *a*-Si:F films can be doped. The dark conductivity of *a*-Si:F increases with spin density, but the photoconductivity is low and independent of the spin density. The differences between *a*-Si:F and *a*-Si:H are interpreted in terms of the different diffusivity and bond strength of fluorine and hydrogen in the *a*-Si matrix. These differences result in a larger density of tail states in *a*-Si:F relative to *a*-Si:H samples of equal spin densities.

I. INTRODUCTION

The interest in fluorinated amorphous silicon (*a*-Si:F) has been stimulated by experimental and theoretical studies which suggested that fluorine may act as a dangling-bond terminator in the amorphous silicon matrix.[1,2] It has been further suggested that *a*-Si:F has better thermal stability than *a*-Si:H, as no fluorine evolution could be detected in annealed *a*-Si:F films up to annealing temperatures close to the crystallization point.[3–6] Amorphous silicon films containing both fluorine and hydrogen (*a*-Si:F:H) have higher deposition rates[4] and were reported to give high doping efficiencies[7] and lower dopant-migration distances than those obtained in *a*-Si:H.[8] The study of the role of fluorine in amorphous silicon is also of interest since the comparison of the results of similar experiments in *a*-Si:F and *a*-Si:H can shed light on the role of hydrogen in amorphous silicon films.

A considerable effort has been devoted to the study of glow-discharge (GD) *a*-Si:F:H and to sputtered (SP) *a*-Si:F without hydrogen.[1–8] Detailed studies of GD *a*-Si:F (with no hydrogen) have not been published despite the fact that plasma glow discharge is the major deposition technique of *a*-Si:H films. The scarcity of data on the properties of Gd *a*-Si:F is partly the result of the inability to obtain *a*-Si:F films from the plasma of commercially available SiF_4 gas. It is possible, though, to produce amorphous silicon films from the plasma of SiF_2 gas. Details of the production of SiF_2 and the deposition of *a*-Si:F films have been published elsewhere, together with some preliminary results on the film properties.[9–11] In the present paper we report on the structural, optical and electronic properties of GD *a*-Si:F films and the dependence of these properties on the deposition temperature (T_d) and annealing temperature (T_a).

A variety of techniques were used for the characterization of the films. *X*-ray diffraction and Raman spectroscopy were used to verify the amorphicity of the films. Nuclear reaction and x-ray photoelectron spectroscopy (XPS) were used to determine the fluorine content in the films. XPS, Auger-electron spectroscopy (AES), and secondary-ion mass spectroscopy (SIMS) were used to determine dopant concentrations and the impurity content. ir spectrophotometry was used to determine the bonding configuration of the fluorine atoms. Spectrophotometry in the visible was employed to determine the effect of the fluorine on the optical gap, E_0. ESR measurements were used to determine the spin density. Thermopower measurements, and dark-conductivity and photoconductivity measurements, were performed as a function of temperature in the range 290—500° K. Finally, microscopic examinations with an interference objective and a scanning electron microscope were performed to detect morphological variations in the annealed films.

We describe first the *a*-Si:F deposition system. Then we describe the film properties and their dependence on the deposition variables. Next, we describe the results of annealing experiments. Finally, we discuss the results, with particular emphasis on the similarities and the differences between *a*-Si:F and *a*-Si:H samples.

II. SAMPLE PREPARATION

Figure 1 illustrates the deposition system of the *a*-Si:F films. SiF_4 gas (from Matheson, Inc.) flows through a mass-flow meter at a typical rate of 2.5 standard cubic centimeters per minute. A needle valve provides a pressure gradient down to the operating pressure of the system. The SiF_4 then flows along 10—15 cm through a charge of silicon cubes cut from a silicon single crystal, held in a fused-silica tube at a temperature of 1120°C. In this furnace, reaction (1) takes place:

$$SiF_4(g)+Si(s)\rightarrow 2SiF_2(g) \quad (1)$$

(g denotes gas; s denotes solid). The gas which exits the furnace is a mixture of SiF_2 and SiF_4 of equal molar ratios,[10,11] and it is transported to the deposition reactor through a glass tube. In typical deposition runs that last-

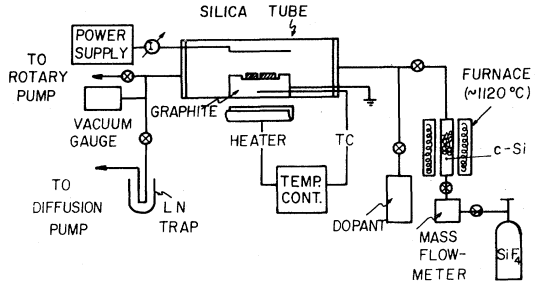

FIG. 1. Schematic representation of deposition system.

ed 120 min, about 200 mg of solid silicon were transported by the SiF_4 gas.

The deposition reactor was a horizontal fused-silica tube 45 mm in diameter. The upper electrode was made of no. 316 stainless steel. The bottom electrode was made of graphite and it served as a radiatively heated sample holder. The upper- and lower-electrode area was 20 and 45 cm^2, respectively, with an interelectrode spacing of 2 cm. Either dc or rf voltages could be coupled to the electrodes. In dc experiments one electrode was held at +530 V and the other electrode was grounded. The dc plasma current at a pressure of 0.15 Torr was 1.2mA, and the plasma just filled the whole interelectrode spacing.

The deposition temperature (T_d) reported below was measured and controlled at the center of the bulk-graphite substrate holder, about 10 mm below its surface. In our system the actual surface temperature T_s was measured during one of the deposition runs using 0.003-in.-diam thermocouple wires spot-welded to a stainless-steel substrate. This gave

$$T_s(^\circ\text{C}) = (0.85 \pm 0.03) T_d + 3^\circ\text{C} \quad (T_d \geq 20^\circ\text{C}) . \qquad (2)$$

The error indicates variations in temperature over the substrate-holder area.

In order to avoid contamination from leaks or from gases desorbed from the walls of the system, it was vacuum-tested before each deposition run. This was done after a pump-down with a diffusion pump, while the reactor was baked at a temperature higher than the anticipated deposition temperature and the silicon furnace was baked at 700 °C. Further purification of the system during deposition was provided by the hot silicon charge itself, which acted as an oxygen getter.[9] The crystalline silicon cubes were etched clean before each deposition.

Dopants were added to the SiF_2+SiF_4 gas mixture past the high-temperature furnace. For n-type doping we usually used pure yellow phosphorus sublimed directly into the gas-flow system from a side branch of the glass tubing. The partial pressure of the phosphorus in the deposition reactor was controlled by varying the temperature of the tube which contained the solid phosphorus chunk. In some experiments we used PF_5 gas from Matheson, Inc. The presence of phosphorus, either obtained by sublimation or in the form of PF_5 gas, increased the deposition rate. p-type doping was done from BF_3 gas. Dopant concentrations reported below were measured in the films by XPS or AES.

In each deposition run we prepared eight samples on (a) fused-quartz substrates for electronic-transport and optical measurements, (b) on silicon wafers (ir grade, from Wacker) for ir, ESR, and electron-spectroscopy measurements, and (c) on no. 316 stainless steel. Four aluminum electrodes with 0.3—,7—, and 14-mm spacings were deposited by vacuum evaporation on top of the samples used for electronic-transport and thermopower measurements.

Occasionally in this paper we compare the results of a-Si:F films to those of a-Si:H films. Wherever we do not quote published results, we refer to a-Si:H films that we deposited in a separate but identical reactor to that used for a-Si:F deposition. Our a-Si:H films were grown from undiluted SiH_4 gas obtained from 3H (Israel). We used similar gas-flow rates in both the F and H systems. The dc plasma voltage in the SiH_4 system needed to obtain uniform plasma glow was 800 V, at a plasma current of 2.3 mA. The rf plasma was operated at the minimum power level required to sustain the plasma.

III. FILM PROPERTIES

A. Structure and composition

Some concern has been expressed recently regarding the amorphicity of doped a-Si:F films.[4] We have verified the amorphicity of the samples reported herein by sampling measurements of x-ray diffraction and Raman scattering. We tested particularly heavily doped samples and samples deposited at elevated temperatures. Since our depositions lasted up to 150 min and the samples might have started to crystallize from the bottom, we checked a few samples by Raman spectroscopy from both the top and bottom side (in the latter case we irradiated the samples through the transparent quartz substrate). We found that all the films either deposited or annealed up to 550 °C were amorphous, as indicated by the absence of a crystalline Raman peak at 521 cm^{-1}. The amorphous Raman peak[12] appeared at (467 ± 8 cm^{-1}, was 80 cm^{-1} wide, and was at least 10 times above noise level in these tests.

The fluorine content of the films was measured by three different techniques. The main tool was XPS analysis using a PHI model 555 instrument. For depth profiling we used AES analysis employing a PHI model 590A system. Both techniques were calibrated by running XPS and AES spectra of eight different a-Si:F samples which were pretested with a nuclear reaction,[19]$F(p,\alpha)^{16}O^*$.[13] Before each XPS or AES measurement we sputtered off, using Ar ions, the thin surface-oxide layer (about 100 Å) which formed on the sample surface in the time interval between film preparation and its measurement. The nuclear test was done with 350-keV protons, which probe the fluorine content at a depth of (1000 ± 250) Å below the surface,[13] and it was unaffected by the surface oxide.

Figure 2 shows an AES depth profile of the fluorine in one of our films. The figure indicates that the fluorine content is nearly uniform as a function of film depth. This film was initially 5900 Å thick. It was completely sputtered off by Ar^+ sputtering during the AES profile measurement, as indicated by the drop of the F signal

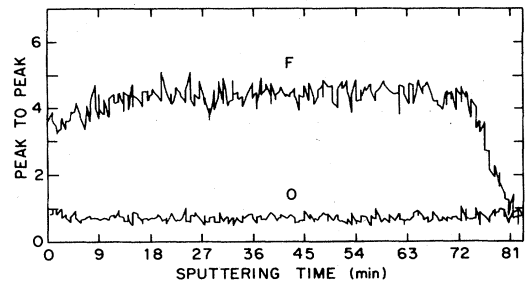

FIG. 2. Depth profile of the fluorine in a dc GD a-Si:F film ($T_d = 250$°C, [F] = 15 at.%, initial film thickness 5900 Å). The film was sputtered off at a rate of 80 Å/min. The figure shows the depth profile starting at a depth of 100 Å (i.e., after the surface oxide was removed).

down to the noise level where the c-Si substrate was exposed. The oxygen signal displayed in Fig. 2 is, in fact, the instrument noise level at the O_{1s} Auger-electron energy, and is equivalent to an upper limit of oxygen concentration of 1000 ppm in the film.

AES and XPS analyses indicated that in nondoped a-Si:F samples, 2000 ppm was the upper limit for any foreign constituent. SIMS analysis, which was done with Ar^+ bombardment in a PHI 590A system with a UTI quadrupole mass spectrometer, did show traces of oxygen. These were of the order of magnitude of the oxygen concentrations found in our a-Si:H films. Since our a-Si:H films performed optically and electronically as high-quality a-Si:H films reported by others (see below), we do not think that these small oxygen inclusions had any appreciable effect on the a-Si:F film properties either.

The left-hand scale of Fig. 3 shows the fluorine content of dc glow-discharge a-Si:F cathode films as a function of deposition temperature, T_d. The fluorine content decreases monotonically with deposition temperature, from about 16 at.% at $T_d = 200$°C to about 2 at.% at $T_d = 600$°C. rf glow-discharge a-Si:F samples contained

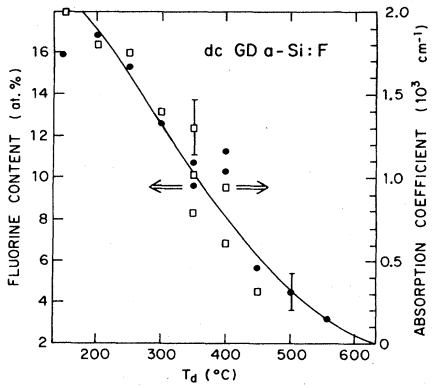

FIG. 3. Fluorine content (●) and the ir-absorption coefficient at the peak of the Si—F stretching band (□) as a function of deposition temperature (dc glow-discharge cathode films on crystalline silicon substrates).

about 60% of the fluorine content of dc cathode samples. The reason for this difference has not yet been clarified.

At $T_d < 150$°C, a thick film of polymeric $(SiF_2)_x$ condensed on the substrates and on the walls of the reactor.[14] This film was transparent to light, and oxidized exothermally upon exposure to air. Because of their chemical composition and instability, films deposited at $T_d < 150$°C are not included in this study.

B. Infrared spectra

Figure 4 shows a typical ir transmission (Tr) spectrum of an a-Si:F film recorded with a Perkin Elmer model 683 double-beam infrared spectrophotometer. A single-crystal silicon substrate was held in the reference beam. A single absorption band can be seen at 820cm^{-1} with a (FWHM) of 25 cm^{-1}. In addition, a broad band around 480 cm^{-1} is observed. The features below 400 cm^{-1} should be disregarded because of instrument noise in this region. The single band at 820 cm^{-1} indicates that the fluorine in this film is bonded predominantly in the Si—F monofluoride form.[14] The broadband around 480 cm^{-1} is the Si TO-phonon mode which becomes ir active due to the polarization of the Si—F bonds. This is the same band seen in Raman spectroscopy.[12]

Similar spectra were obtained for all rf and dc glow-discharge a-Si:F films. The magnitude of the Si-F absorption band decreased monotonically with the fluorine content, as indicated in Fig. 3 (right-hand scale). At $T_d = 500$°C the ir signal of our films got below our detection limit (Tr = ±0.005). Any other absorption peaks in the ir spectrum besides the Si—F monofluorine stretching mode, if present, must have been below our detection limit. This sets an upper limit of about 10% of the total fluorine content of the film in any of the other bonding configurations, Si—F_2, Si—F_3, and Si—F_4. The lack of other features in our ir spectra is remarkable in view of the rich ir spectra, which are obtained in a-Si:F films prepared by sputtering of silicon in the presence of SiF_4 gas.[4–6,15] We have shown elsewhere that the features obtained in sputtered a-Si:F films should be attributed to $(SiF_2)_x$ and SiF_4 species which get trapped in the a-Si films during the sputtering process.[14] It seems that the $(SiF_2)_x$ species are formed at the sputtering target by a process similar to that described by Eq. (1).[16] These species can get trapped in the film even when their inclusion in the film is thermodynamically unfavorable, if another source of silicon of high fluence exists in the pro-

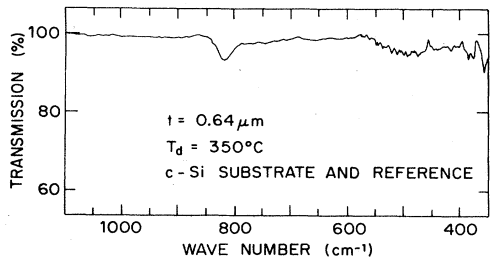

FIG. 4. Infrared spectrum of a dc glow-discharge a-Si:F sample ([F] = 11 at.%).

cess, as in the case of sputtering. The same trapping mechanism causes the trapping of inert Ar atoms in sputtered a-Si films.[17] Such trapping does not seem to occur in the glow-discharge deposition process of a-Si:F films under the deposition conditions described above.

C. Optical band gap

The optical band gap of the a-Si:F samples, E_0, was derived from the formula[18]

$$(\alpha h\nu)^{1/2}=A(h\nu-E_0)\ , \tag{3}$$

where α is the absorption coefficient, $h\nu$ is the photon energy ($h\nu>E_0$), and A is a constant. As has been recently shown, E_0, which is obtained from the extrapolation to $\alpha=0$ of the optical data fitted to Eq. (3), depends on the region of the measured values of α.[19] For the determination of E_0 of our a-Si:F films, we used films of thicknesses in the range 0.1—0.5 μm, with values of α in the range $1.0\times10^5\leq\alpha\leq2.5\times10^5$ cm^{-1}. The E_0 values of dc glow-discharge a-Si:F samples prepared at different deposition temperatures are shown in Fig. 5. It can be seen from the figure that, at $T_d<300$ °C, E_0 increases steeply as the deposition temperature is reduced. From the data of Fig. 3 it can be deduced that E_0 increases when the fluorine content of the film exceeds 12 at.%. On the other hand, at $T_d>300$ °C the optical band gap is almost constant, despite the continuing decrease of the fluorine content of the film with increasing T_d. In fact, in the temperature range, $T_d>300$ °C the optical band gap seems to increase slightly with T_d, reaching the optical properties of anneal-stable, chemical-vapor-deposited (CVD) a-Si films at $T_d\geq550$ °C.[20]

In the region $T_d<300$ °C it seems that the fluorine content dominates the magnitude of the optical band gap. As mentioned above, for a film of 66.6 at.% fluorine [e.g., for a polymeric $(SiF_2)_x$ film] the substance is transparent to visible light, indicating a band gap deep in the ultraviolet energy region. It is expected that, due to the large Si—F bond strength (about 5 eV), the optical gap of a-Si:F will open up as the fluorine content increases. On the other hand, at $T_d>300$ °C the fluorine content seems to be too low to affect the optical band gap. In this region it is more likely that the degree of disorder of the film determines the magnitude of the optical band gap.[21] Thus for $T_d>300$ °C one may presume that the topological disorder decreases with increasing T_d, resulting in a slight increase of E_0.

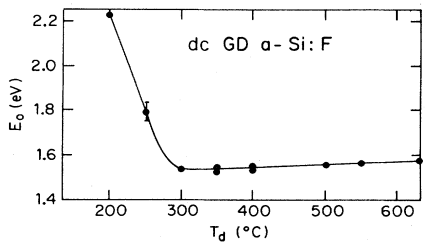

FIG. 5. Optical band gap vs deposition temperature of dc glow-discharge a-Si:F samples (fused-silica substrates; plasma conditions same as in Fig. 3).

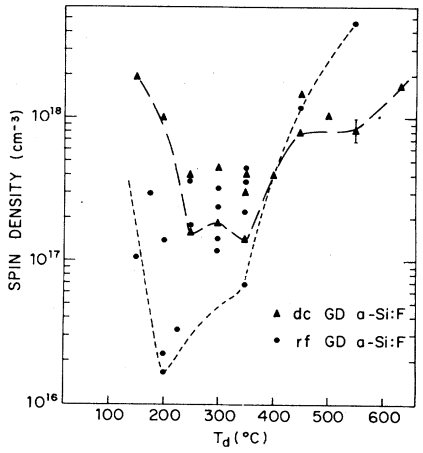

FIG. 6. Spin density vs deposition temperature. The long-dashed and the short-dashed lines give the lowest spin densities achievable in our experiments at the given deposition temperature for dc and rf glow-discharge a-Si:F samples, respectively.

D. Spin density

Electron-spin-resonance (ESR) measurements were made with a Varian Associates EPR-4 instrument. Calibration of the absolute spin density was done at IBM (Yorktown Heights, New York) by comparing a few of our samples to a known c-Si standard. The behavior of the spin density of the a-Si:F films versus deposition temperature was found to be similar to that reported for a-Si:H samples:[22,23] At $T_d\leq150$ °C and $T_d\geq500$ °C, values above 10^{18} spins/cm^3 were obtained, while at $200\leq T_d\leq350$ °C, a region of low spin density was obtained (see Fig. 6). For dc glow-discharge cathode samples the lowest spin-density values were in the range of 2×10^{17} spins /cm^3. These values were obtained for T_d between 250 and 350°C. For rf glow-discharge samples the lowest values were in the range of 2×10^{16} spins/cm^3, and were obtained at deposition temperatures between 200 and 250 °C.

a-Si:H samples prepared in our deposition system at $T_d=250$ °C gave spin densities below 3×10^{16}; some of these films had spin densities below 5×10^{15}cm^{-3}, which was our detection limit for the given sample volume.

The value of the g factor for undoped samples was 2.0055 ± 0.0005, indicating the presence of dangling bonds. The line shape of this ESR signal indicated a symmetric Lorenzian. In doped dc cathode samples the ESR value decreased with dopant content down to levels below our detection limit. This should be attributed to electronic compensation.[24] The g factor changed upon doping in a way similar to that reported for a-Si:H.[24] Details of the effect of doping on the ESR signal in our samples will be published elsewhere.

E. Electronic transport

1. Dark-conductivity measurements

Dark conductivity versus temperature [$\sigma_d(T)$] was measured with planar electrode geometry in a dry, flowing N_2 atmosphere. The applied voltages were between 20 and 40 V over a gap of 0.3 mm. A Keithley model 610C electrometer was used to detect the dark current. The contacts were generally Ohmic after a short 200 °C anneal of the electrodes. This anneal which was performed prior to all electrical measurements was also found necessary in order to desorb humidity and other adsorbates which affected the surface conductivity at resistance values above 10^{10} Ω. Nonlinear I-V curves were found in some nondoped low-spin a-Si:H samples. In these cases we used 4-probe measurements.

Figure 7 shows typical curves of the dark conductivity versus temperature of six a-Si:F samples and one undoped a-Si:H sample. Samples 5—7 had about the same spin densities (at 3×10^{16} spins/cm^3), and their dark conductivities and activation energies are very similar. Samples 3 and 4 had a spin density of 2×10^{17}cm^{-3}. They were prepared under the same conditions as sample 5, but were subsequently annealed (see below). Samples 1 and 2 are phosphorus-doped with a phosphorus content of 0.2 and 2.0 at. %, respectively. The results show, first, a quantitative similarity between the dark conductivity of the low-spin a-Si:F and a-Si:H samples. At higher spin densities, whether obtained by annealing or due to the high deposition temperatures, the dark conductivity of the intrinsic a-Si:F samples increased [from $\sim10^{-10}$ to 5×10^{-7}(Ω^{-1} cm^{-1}) at room temperature], and the activation energy decreased (from ~0.78 to 0.40 eV). Figure 7 also demonstrates the clear increase of the conductivity and the decrease in the activation energy which is obtained in doped a-Si:F samples.

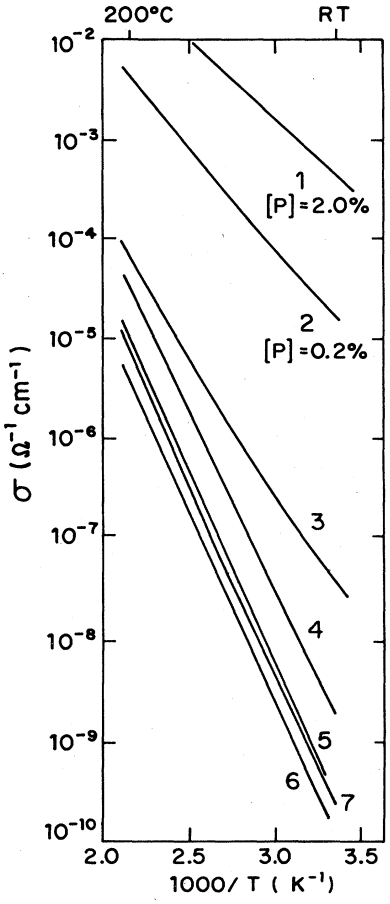

FIG. 7. Dark conductivity vs temperature. Samples 1 and 2: phosphorus-doped dc GD a-Si:F; $T_d=300$ °C. Samples 6 and 5: rf GD a-Si:F; $T_d=200$ and 225 °C, respectively. Samples 4 and 3: same preparation conditions as sample 5; $T_a=325$ and 425 °C, respectively. Sample 7: rf GD a-Si:H; $T_d=250$ °C. RT marks room temperature.

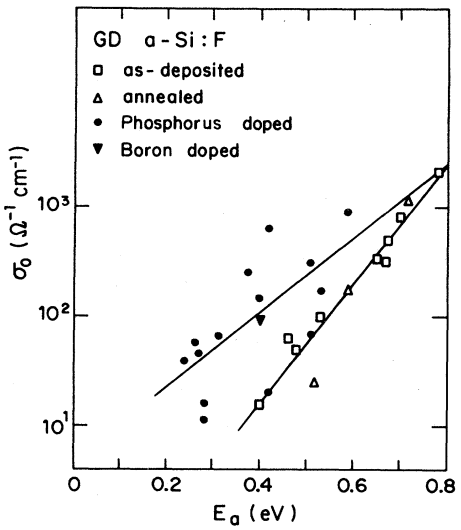

FIG. 8. Pre-exponential factor σ_0 as a function of the activation energy of the dark conductivity.

Figure 8 shows the values of σ_0 versus the activation energy E_a, where σ_0 and E_a are derived from the Arrhenius-like plot (as in Fig. 7) of the conductivity,

$$\sigma_d=\sigma_0\exp(-E_a/k_BT)\ . \tag{4}$$

T is the temperature in °K and k_B is the Boltzmann factor. σ_0 and E_a in Fig. 8 were derived from the conductivity data at $T\geq350$ K, e.g., well above the hopping-conduction region. The figure shows the results for both doped and undoped samples. The results show that the Meyer-Neldel rule holds for a-Si:F as it does for a-Si:H, even though the dependence of σ_0 on E_a in a-Si:F has a smaller exponential coefficient than that reported for a-Si:H.[22] The solid lines in Fig. 8 are the least-squares fits to the data of the doped and undoped samples, respectively. The different experimental points for the doped samples were obtained with different doping levels between 0 and 8 at. % (dopant concentration increasing from right to left). The different experimental points of the nondoped branch were obtained by increasing either T_d or T_a. The optical band gap of all the samples in Fig.

8 was in the range $E_0=(1.58\pm0.07)$ eV. Thus the variations of E_a in the range $0.26\leq E_a\leq 0.78$ eV represent the shift of the Fermi level due either to doping or defect-level formation. Generally, the decrease of E_a in doped samples was associated with *decreasing* spin densities. On the other hand, the decrease of E_a in undoped samples was associated with an *increase* in spin density. In fact, we attribute the larger scatter of the experimental points of the doped samples to the interplay of two mechanisms which shifted E_F, i.e., variations of both dopant- and defect-level concentrations. For the intrinsic samples, on the other hand, only variations of the intrinsic defects (dangling bonds) affect the position of E_F. The two curves in Fig. 8 were found to meet, as expected, for undoped, nonannealed samples. The meeting point is at $E_a=(0.81\pm0.04)$ eV, with $\sigma_0\simeq 2\times10^3\ \Omega^{-1}\ \text{cm}^{-1}$. This indicates that E_a for nondoped, defect-free, *a*-Si:F samples should be 0.81 eV, which marks the position of the Fermi energy for intrinsic *a*-Si:F.

Thermopower measurements showed that nondoped and phosphorus doped *a*-Si:F samples had *n*-type conduction. Boron-doped samples had *p*-type conduction.

2. Photoconductivity measurements

The results reported above for the *a*-Si:F samples show behavior of the structural and electronic properties generally similar to that reported for *a*-Si:H samples. Yet, we found a significant difference between the photoconductivity of *a*-Si:F and that of *a*-Si:H samples. In Fig. 9 we show the photoconductivity versus temperature for some of the samples whose dark conductivity was presented in Fig. 7. The ordinate in Fig. 9 is the product $\eta\mu\tau$, where η is the quantum yield, μ is the mobility, and τ is the mean carrier lifetime. $\eta\mu\tau$ was derived from the photocurrent data by

$$\eta\mu\tau=(i_p h\nu l)/[WeVI_0(1-R)(1-e^{-\alpha d})]\ , \tag{5}$$

where i_p is the photocurrent, l is the interelectrode spacing, W is the electrode width, V is the voltage, I_0 is the incident-light power, R is the sample reflectance, and d is the sample thickness. The light source was a mercury arc lamp chopped at 170 Hz, filtered with a 5461 Å interference filter. The light power I_0 was 25 mW/cm^2 (7×10^{16} photons/cm^2), except for curve (b) of sample 7, which was obtained with $I_0=0.25$ mW/cm^2. The photocurrent was amplified by a Princeton Applied Research (PAR) model 184 current-sensitive preamplifier and a PAR model 114 signal-conditioning amplifier, and then fed in parallel to a Tektronix oscilloscope and an Ithaco model 391A lock-in amplifier. Experimental points on the photocurrent curve were obtained while going from high toward low temperatures, using short exposures ($\sim$ 30 sec). The temperature was varied in the dark. This was done in order to avoid the Staebler-Wronsky effect,[22] even though this effect was found to be very small in our nondoped *a*-Si:H films, and undetectable in our *a*-Si:F films.

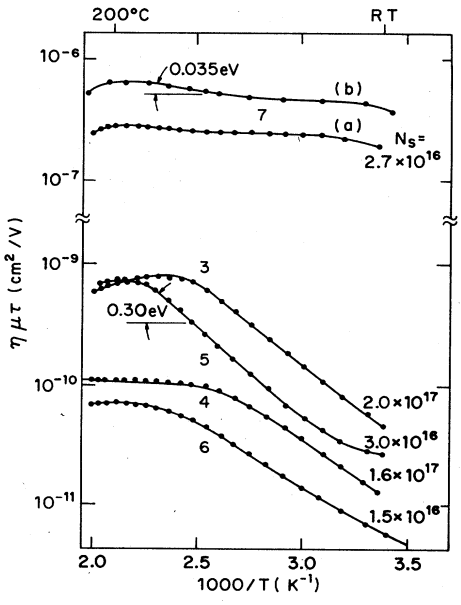

FIG. 9. Photoconductivity of rf glow-discharge *a*-Si:H and *a*-Si:F samples (photon flux 7×10^{16} cm^{-2}sec^{-1}; except for curve (b), photon flux 7×10^{14} cm^{-2}sec^{-1}. $\lambda=5461$ Å, dry-N_2 atmosphere, 400 V/cm).

From Fig. 9 it can be seen, first, that at room temperature the intrinsic *a*-Si:F samples have a photocurrent which is some 4 orders of magnitude lower than that of the *a*-Si:H sample photocurrent. The photocurrent we obtained for our nondoped *a*-Si:H samples was similar to that reported for bipolar *a*-Si:H samples by other workers.[25] Curve (a) has the same main features as curve (b) taken with 2 orders of magnitude less light intensity. This shows that the lack of activation energy in curve (a) is not due to some saturation effect. The higher value of $\eta\mu\tau$ in curve (b) is attributed to a higher value of τ. The values of $\eta\mu\tau$ we obtained for the *a*-Si:F samples were in the range between 5×10^{-12} and 5×10^{-10} cm^2/V. No clear correlation could be found between the values of $\eta\mu\tau$ and the deposition conditions. Furthermore, the photoconductivity values we obtained in the nondoped *a*-Si:F samples were found to be independent of spin density for $N_s\leq10^{18}\text{cm}^{-3}$, even though σ_0 and E_F were shown above to depend on the spin density. The photocurrent of the *a*-Si:F samples could be increased by up to 3 orders of magnitude by phosphorus doping, but this was still far below the photocurrent of doped *a*-Si:H samples.[25]

Another significant point seen in Fig. 9 is the difference in the temperature dependence of the photocurrent of the *a*-Si:F and *a*-Si:H samples. The slope of the photocurrent versus temperature on the semilogarithmic scale gave activation energies between 0.22 and 0.30 eV for the *a*-Si:F samples, and much lower values—of the order of 0.04 eV—for the *a*-Si:H samples. In fact, as can be seen from Fig. 9, the use of the term "activation energy" is inappropriate for sample 7 since no clear exponential dependence of the photocurrent on temperature is obtained; the slope of $\eta\mu\tau$ in Fig. 9 for the *a*-Si:H sample is only given for the sake of comparison to the *a*-Si:F samples. The activation energy of the photoconductivity of the *a*-Si:H samples below room temperature (down to -70 °C) was 0.11 eV, which was, still, much less than that of the *a*-Si:F samples.

IV. ANNEALING EXPERIMENTS

Annealing experiments are a useful technique in the study of *a*-Si:F (as well as *a*-Si:H) samples. By driving the halogen atoms out of their positions in the film and measuring the resultant film properties, one can deduce what the role of the halogen atoms was in the preannealed film.

Below, we report the results of annealing experiments of *a*-Si:F samples whose initial (as-deposited) spin density was about 2×10^{16} cm^2. The *a*-Si:F samples reported here are GD rf samples prepared at $T_d=225$ °C. They were annealed *in situ* at the end of each deposition run. Deposition time was 150 min and the annealing period was 15 min. The deposited samples contained about 8 at.% fluorine. It should be noted that different annealing temperatures correspond to different deposition runs, which causes some scatter of the experimental results. Samples prepared below 200 °C could not be annealed without major damage to the films, which cracked and peeled off. In the data presented below, the 200 and 225 °C data points belong to nonannealed samples prepared at the listed temperatures.

Figure 10 shows the spin density of the samples as a function of annealing temperature. The spin density increases from 1.5×10^{16} spins/cm^3 for the nonannealed sample, up to 4×10^{18} cm^{-3} at $T_a=520$ °C. In one of our rf glow-discharge *a*-Si:F samples that was subjected to successive isochronal anneals at temperature intervals of 50 °C we found a result very similar to the solid curve plotted in Fig. 10. The maximum value of the spin density on that sample was obtained at $T_a=630$ °C. Beyond $T_a=630$ °C the ESR dropped sharply as the film started to crystallize.

The monotonic increase of the ESR signal in our rf GD *a*-Si:F samples indicates that Si—F bond breaking takes place at all temperatures above the deposition temperature. Bond reconstruction does not seem to keep pace with bond breaking, particularly at low annealing temperatures. Furthermore, the fluorine in the film does not seem to diffuse efficiently to the locations of the dangling bonds formed. This is somewhat different than the case of *a*-Si:H, where the spin density does not start to increase before annealing temperatures of 250—300 °C have been reached and a few atomic percent of hydrogen has evolved.[26–28] Nevertheless, the saturation value of the spin density in annealed *a*-Si:H samples is the same as in *a*-Si:F, e.g., about 4×10^{18} cm^{-3}, and it is obtained at $T_a\approx600$ °C.

Figure 11 shows the dark conductivity of the *a*-Si:F samples at room temperature as a function of annealing temperature. From Figs. 10 and 11 we see that the dark conductivity of the annealed samples increases with spin density. At spin densities above 10^{18} cm^{-3}, the dark conductivity saturates at a value of 3×10^{-7} Ω^{-1}cm^{-1}. As mentioned before, we also found a corresponding decrease of E_a with increasing spin density, from 0.78 eV at a spin density of 1.5×10^{16} cm^{-3} to 0.5 eV at a spin density of 4×10^{18} cm^{-3}. The results indicate the strong correlation between the transport properties of equilibrium charge carriers in undoped films and the spin density of the samples: When the density of spin defects increases, the Fermi level gets closer to the conduction band, thereby increasing the conductivity.

Figure 12 shows the room-temperature photoconductivity of the samples of Fig. 11. As mentioned before, no correlation could be found between the photoconductivity and the spin density of the samples. This is strikingly different than what one finds in *a*-Si:H; Jones *et al.* report a variation of 4 orders of magnitude in the photoconductivity of *a*-Si:H when the films are annealed from $T_a=400$ °C to $T_a=600$ °C.[29] Over that range, the spin density changes from 2×10^{16} to 4×10^{18} cm^{-3}.[28]

Our ir-transmission studies indicated that, during annealing at temperatures above the sample deposition tem-

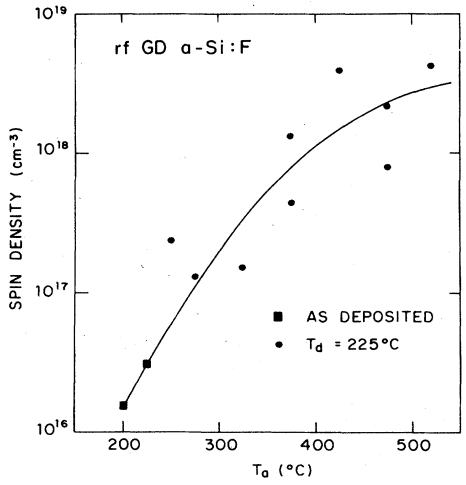

FIG. 10. Spin density vs annealing temperature.

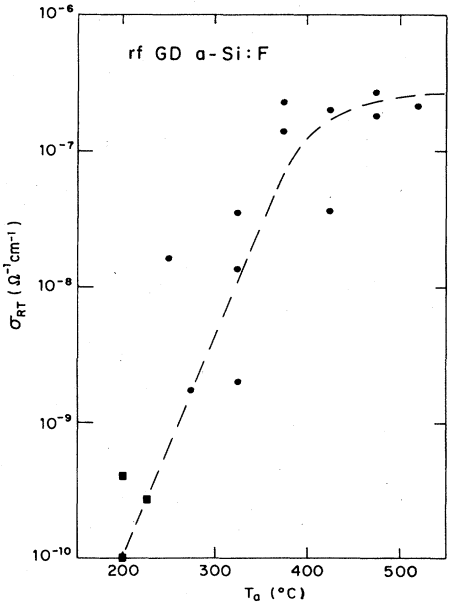

FIG. 11. Room-temperature dark conductivity vs annealing temperature. Same deposition and annealing conditions as in Fig. 10.

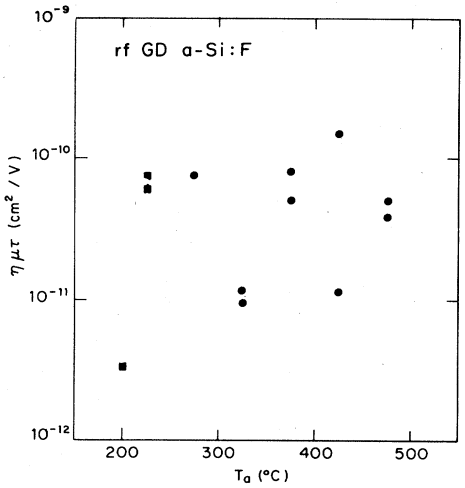

FIG. 12. Room-temperature photoconductivity vs annealing temperature. Same deposition and annealing conditions as in Fig. 10.

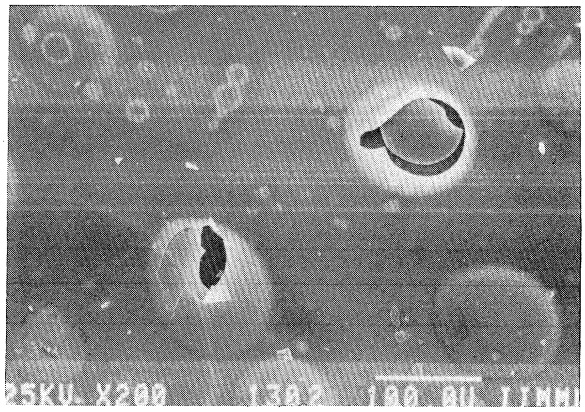

FIG. 13. SEM micrograph of exploded bubbles in an annealed a-Si:F sample ($T_a = 750\,°C$). The bubble diameter is about 50 μm, and it built up between the film and the substrate.

perature, the fluorine in the film was transformed from Si—F bonds into SiF_4 gas molecules.[14,30] These gas molecules did not effuse out of the film, but were trapped in bubbles between the film and the substrate. Only at annealing temperatures above 600 °C did these bubbles explode and their SiF_4 gas content erupt.[3–6,30] Figure 13 shows a scanning-electron-microscope (SEM) micrograph of an annealed film with bubbles in formation and two exploded bubbles. The evolution of fluorine mostly by violent mechanical destruction of the film indicates, unlike hydrogen in a-Si:H, that fluorine has no easy diffusion channels out of the a-Si film.

V. DISCUSSION

Let us summarize the main findings on a-Si:F and compare them to the results obtained in a-Si:H samples. Eliminating the complexity of the gas-transport process, a-Si:F films can be produced in a way similar to that of a-Si:H films, either by rf or dc glow-discharge decomposition of a silicon-halogen plasma. The films can be prepared with spin densities of the order 10^{16} cm^{-3}. Upon annealing to 600 °C, their spin density increases to about 4×10^{18} cm^{-3}. Their dark conductivity is closely tied to their spin density: the higher the spin density, the lower the thermal activation energy, and also the larger the hopping-conduction contribution at low temperatures. The activation energy of low-spin, nondoped samples is about 0.8 eV, and their dark conductivity at room temperature is about $10^{-10}\,\Omega^{-1}\,\text{cm}^{-1}$, with carrier transport in extended states. The above findings indicate that both a-Si:F and a-Si:H are amorphous materials of relatively "clean" band gaps. Fluorine clearly compensates for dangling bonds and reduces the density of deep gap states, as indicated by the ESR and dark-conductivity measurements.

There are, though, some differences between glow-discharge a-Si:F and a-Si:H samples, which we now enumerate.

(1) While the ir spectrum of a-Si:H indicates several forms of hydrogen bonding to silicon, e.g., Si—H, Si—H_2, Si—H_3, or $(SiH_2)_x$, [22,28] in glow-discharge a-Si:F we find the fluorine predominantly in Si-F monofluoride bonds. This is independent of deposition temperature (for $T_d > 150\,°C$), of plasma conditions, or of fluorine content.

(2) The optical gap of a-Si:F does not seem to depend on the fluorine content at fluorine concentrations below 12 at. %. In a-Si:H, on the other hand, the gap increases significantly with H content.[22]

(3) The photoconductivity of nondoped a-Si:F films at room temperature is 3—4 orders of magnitude lower than that of a-Si:H films. The comparison is done for samples prepared in similar reactors which have similar spin densities and similar dark conductivities.

(4) The thermal activation energy of the photoconductivity of a-Si:F is between 0.22 and 0.30 eV, much higher than that of intrinsic a-Si:H.

(5) Upon annealing at $T_a > T_d$, the hydrogen in a-Si:H diffuses (atomically) and evolves from the free surface. In a-Si:F the fluorine forms stable SiF_4 molecules that accumulate in trapped bubbles. The bubbles grow, probably by a mechanism of defect diffusion.

(6) The spin density of rf glow-discharge a-Si:F samples increases sharply with annealing temperature for $T_a > T_d$, even at T_a as low as 225 C, while in a-Si:H there is a temperature range in which the spin density decreases as the annealing temperature is raised.

We thus find that in some respects (ESR versus T_d, dark transport) fluorine has the same effect as hydrogen in the a-Si matrix, while in other respects (optical gap at [F] < 12 at. %, photoconductance) the films behave as if there was no fluorine present at all.

Let us discuss first the photoconductivity of a-Si:F. Even though there is as yet no single accepted model for the temperature dependence of the steady-state photoconductivity in amorphous semiconductors, it is generally accepted that the increase in the photocurrent with temperature at temperatures below the photocurrent maximum arises from thermal excitations of photocarriers which are trapped in the shallow band-tail states.[31–34] Thus, the

higher activation energy and the lower value of the photocurrent of *a*-Si:F with respect to *a*-Si:H are consistent with the assumption that the density of tail states in *a*-Si:F is much larger and penetrates much deeper into the mobility gap than it does in *a*-Si:H.

To test the hypothesis of the wider band tail in *a*-Si:F, we recently performed photoinduced-absorption (PA) measurements.[35] As analyzed by Tauc,[36] the PA experiment probes the density of trapped photocarriers in the band tails of the amorphous semiconductor. We found that near room temperature the magnitude of the PA signal in *a*-Si:F is about 2 orders of magnitude higher than that of *a*-Si:H.[35] This result is consistent with the assumption that, indeed, the larger density of tail states in *a*-Si:F is the origin of the low macroscopic mobility and the low photoconductivity of that material. The large density of tail states can also explain the independence of the photoconductivity of *a*-Si:F on the spin density: With a sufficiently high density of tail states, as is obtained in *a*-Si:F, tail-to-tail recombination may dominate, and then the recombination through spin centers becomes insignificant. There also seems to be some evidence[37] that, even in *a*-Si:H, recombination is dominated by tail states and not by dangling bonds.

The optical band gap in *a*-Si:F was found to be practically independent of the density of spin defects, as shown above. Others have shown that the optical band gap in *a*-Si:H, as derived from Eq. (3), is directly related to the density of tail states and the topological disorder of the film.[21] We thus conclude that in *a*-Si:F, unlike in *a*-Si:H, the density of tail states is always high, independent of the degree of compensation of deep defect states by the fluorine. We also see that variations in the fluorine content (below $\sim$ 10 at. %) do not affect the optical gap and hence have little effect on the high topological disorder. However, our annealing experiments show that the fluorine content has a strong effect on the ESR signal.

As to the origin of the large difference between the density of tail states of low-spin *a*-Si:F and *a*-Si:H samples, we note that the band-tail states in amorphous semiconductors are attributed to the local potential fluctuations in the disordered system.[31] One possible origin for the potential fluctuations is the local strain of the chemical bonds that cannot achieve their relaxed bond lengths and angles. We may thus assume that hydrogen has the ability to relax the strained bonds, while fluorine in *a*-Si:F does not. It was indeed suggested previously that the special feature of hydrogen in *a*-Si:H is to reduce the strain by reducing the average coordination number of the overconstrained disordered tetrahedral structure.[38,39] However, the reduction of the average coordination number is definitely not the clue to the low density of tail states in *a*-Si:H, since similar amounts of fluorine and hydrogen in the amorphous silicon matrix, which reduce the average coordination number by exactly the same amount, give very different densities of tail states in the two materials, as shown above.

We thus propose that the special feature of hydrogen lies in the strength of its bond to the silicon atom. We note that the Si—H bond strength (3.09 eV) is slightly lower and almost equal to the Si—Si bond strength (3.29 eV).[40] On the other hand, the Si—F bond strength is much higher (5.30 eV).[40] (These values are for diatomic molecules; in the solid all bonding energies are expected to increase slightly due to the different electronegativity of the bonded silicon.) We also note that hydrogen diffusion and evolution experiments have indicated that the hydrogen in *a*-Si:H is bonded in pairs at sites of neighboring silicon atoms in the form[41,42]

$$a\text{-Si}\equiv\text{Si—HH—Si}\equiv a\text{-Si} \; . \tag{6}$$

Combining the information on the bond strength of hydrogen and fluorine to silicon and the special bonding form of hydrogen in pairs, we propose that hydrogen is unique in its ability to attack, and dissociate preferentially, strained Si—Si bonds. It does so by hopping from site to site, ending at points of strained bonds, where its presence helps best to reduce the free energy of the system. These ending points seem paired as given by Eq. (6). Since the bond strength of Si—H is somewhat less than that of Si—Si, hydrogen selectively dissociates strained Si—Si bonds whose contribution to the total free energy is high. In this way the atomic scale potential fluctuations are reduced to a minimum and the tail states are eliminated. Fluorine, on the other hand, is not selective to strained Si—Si bonds and it does not dissociate them preferentially. Instead, it bonds at random in the *a*-Si matrix, because *any* bond of fluorine to silicon considerably reduces the free energy of the system. The process which further lowers the free energy in the Si-F system is not the migration of the fluorine to sites of strained silicon bonds, but rather the formation of stable SiF_4 molecules.[43,44] Indeed, upon annealing of *a*-Si:F films, we found that the Si—F bonds are replaced by SiF_4 molecules. This process, of course, consumes the fluorine atoms of *a*-Si:F without helping to relieve the strained bonds.

We do not believe that the higher density of tail states in *a*-Si:F should be attributed to defects associated with the size of the fluorine versus that of the hydrogen atom. That is because, first, the bond length of Si—F is very close to that of Si—H (1.53 versus 1.47 Å),[40] and, second, *a*-Si:F:H films were found to perform electronically in a way similar to that of *a*-Si:H without fluorine.[4,7] If the fluorine itself was the origin of the defects in *a*-Si:F, these defects should have also been found in *a*-Si:F:H. We thus conclude that the high density of tail states and the low photoconductivity of *a*-Si:F are not due to a specific property of fluorine, but rather to a specific property it lacks, that is, the ability to relieve strained bonds.

Our model implies that the *a*-Si:F should be more strained than the *a*-Si:H. A measure of the strain in amorphous silicon can be obtained from the width of the Raman TO band observed in *a*-Si.[45] Shimizu *et al.*[46] have found that sputtered *a*-Si:F samples had higher strain than sputtered *a*-Si:H. We have performed preliminary Raman experiments on our glow-discharge *a*-SiF and *a*-Si:H and also have evidence that the *a*-Si:F is more strained than *a*-Si:H.

Our results also suggest a different view of the NMR studies of GD *a*-Si:H. These studies have shown that the NMR signal of *a*-Si:H is composed of a narrow and a broad line.[38,47] The narrow component was attributed to

hydrogen scattered in silicon grains and the broad line was assumed to belong to a "tissue material" of higher hydrogen density. We propose that the scattered monohybride has a function similar to that of fluorine in *a*-Si:F it does help to cancel deep traps and spins, but not shallow traps. The hydrogen which exhibits the unique property is indeed the hydrogen of the strain-relieving pairs (SRP's), which helps to eliminate the shallow traps. The SRP's contribute to a broad NMR line since the separation between two hydrogen atoms of an SRP can easily be smaller than 1.9 Å because the interatomic distance of relaxed Si—Si bonds is 2.3 Å.[40] The value 1.9 Å, derived from the NMR data,[47] is an upper limit of the separation of a pair of H atoms in an SRP if the pairs are to be dispersed in the material and are to account for the broad NMR line.[47] [NMR experiments in *a*-Si(F,H) and sputtered *a*-Si:F also show a broad line.[38] However, the broad line in sputtered *a*-Si:F should be attributed to the presence of SiF_4 molecules, not to fluorine SRP's. SiF_4 molecules exist in large quantities in sputtered *a*-Si:F and *a*-Si:F:H films.[6]]

In conclusion, we have shown that *a*-Si:F films of low spin density can be produced, can be doped, and that their optical properties and dark conductivity are similar to those of *a*-Si:H samples. We show, however, that the density of the electronic tail states of *a*-Si:F penetrates much deeper into the forbidden band gap. As a result, the photoconductivity of *a*-Si:F is lower and its photoinduced absorption signal is higher than that of *a*-Si:H. We have shown that the photoconductivity in *a*-Si:F is independent of the spin density of the films, and we have argued that also in *a*-Si:H the low photoconductivity of annealed samples may be, to a large extent, the result of an increased density of tail states. Thus the high photoconductivity of good-quality *a*-Si:H samples is the result of the low density of shallow tail states in this disordered material. We suggest that this is due to structural strain relief, which reduces the local potential fluctuations which are responsible for the tail states. We have argued that the structure relaxation in *a*-Si:H is not a consequence of the slightly reduced coordination number, but a special property of the Si:H system related to the diffusivity of hydrogen and the thermodynamics of the Si:H system. We have argued that due to the high bond strength of Si—F and the poor diffusivity of elemental fluorine in the *a*-Si:F matrix, no strain relief can be obtained in the *a*-Si:F system, even though the material can be prepared so as to give low spin density.

Finally, our results imply that, if one could produce an intrinsic continuous random network of a tetrahedral amorphous material with no spins and no hydrogen or fluorine, as suggested by Paul,[48] that material would not perform like low-spin *a*-Si:H samples. In fact, such hypothetical material may have low room-temperature dark conductivity, activation energy which is about half the band gap, and negligible phonon-assisted tunneling conduction. Yet, it would probably have poor photoconductivity due to a large density of strain-induced tail states. Our low-spin *a*-Si:F films seem to be close to that hypothetical material.

Note added. Recently, measurements were made on our samples by Dr. M. Stutzmann at the Xerox Palo Alto Research Center. These measurements indicate that, as compared to the Xerox standards, all spin densities reported in this paper should be higher by an order of magnitude.

ACKNOWLEDGMENTS

We would like to thank Dr. J. Reimer (IBM, Yorktown Heights, New York) for the ESR calibration measurements of a few of our samples, Dr. Z. Vardeni for the photoabsorption measurements, Professor R. Kalish for the nuclear test determination of fluorine content, and Dr. R. Brener for the XPS, AES, and SIMS analyses. The technical support of Mrs. L. Patlagin and Mr. A. Kessel in sample preparation, and of Mrs. R. Hida, Mr. P. Ron, and Mr. L. Frey in sample characterization is gratefully acknowledged. This research was supported by grants from the National Council for Research and Development, Israel, and the Kernforschungsanlage Jülich, West Germany, and by the Fund for Promotion of Research at the Technion.

[1]S. R. Ovshinsky and A. Madan, Nature (London) **276**, 483 (1978).

[2]R. Fisch and D. C. Licciardello, Phys. Rev. Lett. **41**, 889 (1978).

[3]H. Matsumura, Y. Nakagome, and S. Furukawa, Appl. Phys. Lett. **36**, 439 (1980); Y. Nakagome, H. Matsumura, and S. Furukawa, Jpn. J. Appl. Phys. **19**, L87 (1980).

[4]H. Matsumura and S. Furukawa, in *Amorphous Semiconductor Technology and Devices,* edited by Y. Hamakawa (North-Holland, Amsterdam, 1982), pp. 88—108.

[5]K. Yamamoto, M. Tsuji, K. Washio, H. Kasahara, and K. Abe, J. Phys. Soc. Jpn. **52**, 925 (1983).

[6]C. J. Fang, L. Ley, H. R. Shanks, K. J. Gruntz, and M. Cardona, Phys. Rev. B **22**, 6140 (1982).

[7]A. Madan, S. R. Ovshinsky, and E. Benn, Philos. Mag. B **40**, 259 (1979).

[8]H. Matsumura and S. Furukawa, Jpn. J. Appl. Phys. **22**, 523 (1983).

[9]M. Janai, R. Weil, K. H. Levin, B. Pratt, R. Kalish, G. Braunstein, M. Teicher, and M. Wolf, J. Appl. Phys. **52**, 3622 (1981).

[10]M. Janai, S. Aftergood, R. B. Weil, and B. Pratt, J. Electrochem. Soc. **128**, 2660 (1981).

[11]R. Weil, M. Janai, B. Pratt, K. H. Levin, and F. Moser, J. Phys. (Paris) Colloq., Suppl. 10, **42**, **C4—643** (1981).

[12]J. F. Morhange, R. Beserman, and M. Balkanski, Phys. Status Solidi A **23**, 383 (1974).

[13]F. Moser, M. Janai, R. Weil, B. Pratt, R. Kalish, K. Levin, and R. Brener, Thin Solid Films **90**, 161 (1982).

[14]M. Janai, L. Frey, R. Weil, and B. Pratt, Solid State Commun. **48**, 521 (1983).

[15]T. Shimada, Y. Katayama, and S. Horigome, Jpn. Appl. Phys.

19, L265 (1980); T. Shimada and Y. Katayama, in Proceedings of the 15th International Conference on the Physics of Semiconductors [J. Phys. Soc. Jpn. Suppl. A **49**, 1245 (1980)].

[16]Y. Y. Tu, T. J. Chuang, and H. F. Winters, Phys. Rev. B **23**, 823 (1981).

[17]K. Tanaka, S. Yamasaki, N. Nakagawa, A. Matsuda, H. Okhushi, M. Matsumura, and S. Iizima, J. Non-Cryst. Solids **35—36**, 475 (1980).

[18]J. Tauc, in *Optical Properties of Solids,* edited by F. Abeles (North-Holland, Amsterdam, 1970).

[19]G. D. Cody, C. R. Wronski, B. Abeles, R. B. Stephens, and B. Brooks, Sol. Cells **2**, 227 (1980); G. D. Cody, B. G. Brooks, and B. Abeles, Sol. Energy Mater. **8**, 231 (1982).

[20]M. Janai, D. D. Allred, D. C. Booth, and B. O. Seraphin, Sol. Energy Mater. **1**, 11 (1979).

[21]H. Fritzsche, Sol. Energy Mater. **3**, 447 (1980).

[22]G. D. Cody, T. Tiedje, B. Abeles, T. D. Moustakas, B. Brooks, and Y. Goldstein, J. Phys. (Paris) Colloq., Suppl. 10, **42**, **C4**-301 (1981); G. D. Cody, T. Tiedje, B. Abeles, B. Brooks, and Y. Goldstein, Phys. Rev. Lett. **47**, 1480 (1981); G. D. Cody, B. Abeles, B. Brooks, P. Persans, C. Roxlo, A. Ruppert, and C. Wronski, J. Non-Cryst. Solids **59-60**, 325 (1983); V. Grasso, A. M. Mezzasalma, G. Moudio, and F. Meri, Nuovo Cimento **1D**, 841 (1982).

[23]H. Fritzsche, C. C. Tsai, and P. Persans, Solid State Technol. **21**, 55 (1978).

[24]J. Magarino, D. Kaplan, A. Friederich, and A. Deneuville, Philos. Mag. B **45**, 285 (1982).

[25]P. E. Vanier, Sol. Cells **9**, 85 (1983).

[26]W. Beyer and H. Wagner, J. Non-Cryst. Solids **59-60**, 161 (1983).

[27]D. K. Biegelsen, R. A. Street, C. C. Tsai, and J. C. Knights, Phys. Rev. B **20**, 4839 (1979).

[28]C. C. Tsai, H. Fritzsche, M. H. Tanielian, P. J. Gaczi, P. D. Persans, and M. A. Vesaghi, in *Proceedings of the 7th International Conference on Amorphous and Liquid Semiconductors,* edited by W. Spear (Center for Industrial Consultancy and Liaison, University of Edinburgh, Edinburgh, 1977), p. 339.

[29]D. I. Jones, R. A. Gibson, P. G. Le Comber, and W. E. Spear, Sol. Energy Mater. **2**, 93 (1979).

[30]M. Janai, R. Weil, and B. Pratt, J. Non-Cryst. Solids **59-60**, 743 (1983).

[31]N. F. Mott and E. A. Davis, *Electronic Processes in Non-Crystalline Materials,* 2nd ed. (Clarendon, Oxford, 1979).

[32]W. E. Spear and P. G. Le Comber, in *Photoconductivity and Related Phenomena,* edited by J. Mort and D. M. Pai (Elsevier, New York, 1976), pp. 185—214.

[33]W. E. Spear, H. Al-Ani, and P. G. Le Comber, Philos. Mag. B **43**, 781 (1981).

[34]R. A. Street, Solid State Commun. **39**, 263 (1981); R. A. Street, J. Phys. (Paris) Colloq., Suppl. 10, **42**, C4-575 (1981).

[35]M. Janai, Z. Vardeni, R. Weil, B. Pratt, and M. Olshaker, in *Optical Effects in Amorphous Semiconductors (Snowbird, Utah, 1984),* edited by P. C. Taylor and S. G. Bishop (AIP, New York, 1984), pp. 364—370.

[36]J. Tauc, in *Festkörperproblems XXII* (Advances in Solid State Physics), edited by P. Grosse Aachen (Vieweg, Braunschweig, 1982), Vol. 22, p. 85.

[37]D. R. Wake and N. M. Amer, Phys. Rev. B **27**, 2598 (1983).

[38]T. Shimizu, J. Non-Cryst. Solids **59-60**, 117 (1983).

[39]R. Zallen, *The Physics of Amorphous Solids* (Wiley, New York, 1983), p. 291.

[40]J. A. Kerr and A. F. Trotman-Dickenson, in *CRC Handbook of Chemistry and Physics, 53rd ed. (Chemical Rubber Company,* Akron, Ohio, 1973), p. F-183.

[41]M. Y. Ching, D. J. Lam, and C. C. Lin, Phys. Rev. B **21**, 2378 (1980).

[42]W. Beyer and H. Wagner, J. Non-Cryst. Solids **59-60**, 161 (1983).

[43]H. Boyd and M. S. Tang, Solid State Technol. **22**, 133 (1979).

[44]D. L. Flamm, Solid State Technol. **22**, 109 (1979).

[45]J. S. Lannin, L. J. Pilione, S. T. Kshirsagar, R. Messier, and R. C. Ross, Phys. Rev. B **26**, 3506 (1982).

[46]A. Morimoto, S. Oozora, M. Kumeda, and T. Shimizu, Solid State Commun. **47**, 773 (1981).

[47]J. A. Reimer, R. W. Vaughan, and J. C. Knights, Phys. Rev. Lett. **44**, 193 (1980); Phys. Rev. B **24**, 3360 (1981).

[48]W. Paul, J. Phys. (Paris) Colloq., Suppl. 10, **42**, C4-1165 (1981).

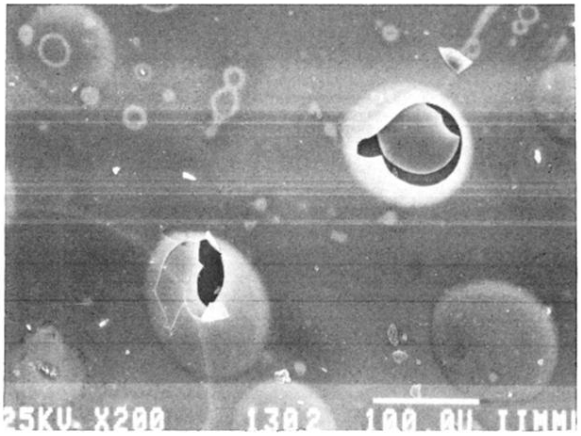

FIG. 13. SEM micrograph of exploded bubbles in an annealed a-Si:F sample ($T_a = 750\,^{\circ}\mathrm{C}$). The bubble diameter is about 50 μm, and it built up between the film and the substrate.